Bi-Fidelity Modeling of Geometric Impact on NACA Airfoil Performance

Ryan Skinner[1]

[1]University of Colorado, Boulder, CO USA

Abstract

This bi-fidelity investigation explores the effect of variation in geometry and angle of attack on the performance of a 2-D NACA 4412 airfoil. The flow is incompressible and is characterized by a Reynolds number of 3 million. All simulations rely on the steady Spalart-Allmaras (SA) RANS turbulence closure. Low-fidelity simulations use a coarse mesh with unresolved boundary layers (BLs), whereas high-fidelity simulations employ a refined mesh that fully resolves the near-wall BL. Predictive capacity of the bi-fidelity approach is analysed with pressure coefficient data.

1 Introduction and Motivation

The need to characterize and optimize the design of unsteady aerodynamic systems becomes more pressing as atmospheric vehicles push performance boundaries. Despite advances over the last five decades in turbulence modeling, accurately capturing the relevant dynamics is prohibitively expensive in the context of uncertainty quantification (UQ) and design optimization (DO). The finite time to market for most high-performance aerospace products constrains simulations' quantity and rigor, and can lead to uncertain and sub-optimal performance. Any method that ameliorates this problem is directly applicable to industry.

The bi-fidelity approach seeks to address the shortcomings of traditional brute-force UQ/DO strategies. Bi-fidelity modeling has two steps. First, a number of low-fidelity (LF) simulations are run. LF simulations do not capture the exact physics of the system, but place low demand on computational resources. These LF realizations are used to generate both an interpolation and a low-rank approximation of a solution quantity as a function of design parameters. For aerodynamics, LF simulations may employ less stringent numerical convergence criteria, coarser meshes, or less-accurate turbulence models. Second, high-fidelity (HF) simulations are run for each combination of parameters deemed important by the low-rank approximation. HF simulations are ideally as accurate as possible, addressing all shortcomings of the LF model. The HF results are used in conjunction with the low-fidelity interpolating coefficients to approximate the solution response over the parameter space.

Though 2-D NACA airfoils command little topical interest, this family is nonetheless selected for two reasons. First, it is a standard academic geometry that was thoroughly studied in the 1930s and '40s, resulting in readily-available validation data (see NACA reports 563, 613, and 824). Second, applying the bi-fidelity approach to a NACA airfoil offers a proving ground for the method and analysis tools, which can be scaled up to more industrially-relevant systems in future work. Ultimately, this technology will expanded to multi-fidelity simulations of flow over complex engineering geometries, such as a multi-element airfoil at high angle of attack or active flow control in an aggressive subsonic diffuser.

1.1 Problem Statement

The present work seeks to quantify the effect of variability in geometric parameters defining a NACA 4-digit series airfoil on the C_p distribution across its surface. Specifically, we consider maximum camber m, location of maximum camber p, maximum thickness t, and angle of attack α. All but α are specified as a fraction of the chord c, which we take to be unity.

2 Solution Approach

2.1 Flow Simulation

Simulations are run in PHASTA, the parallel hierarchic adaptive stabilized transient analysis CFD code developed and maintained by Prof. Kenneth Jansen's group at the University of Colorado at Boulder. The compressible branch is used solely to carry out the mesh deformation, and the incompressible branch is used to actually run the simulation. The lack of PETSc integration in the incompressible formulation necessitates this workflow.

A schematic of the computational fluid domain is shown in Figure 1. It has streamwise length $L = 60$ m, vertical height $H = 10$ m, and span-wise width $W = 0.01$ m. These dimensions correspond to Cartesian directions x, y, and z. The airfoil's chord is 1.0 m, and its leading edge is located 15 m upstream from the inflow and equidistant from the top and bottom walls.

Simulations are incompressible, target a Reynolds number of 3 million with respect to the airfoil chord, and use the Spalart-Allmaras (SA) RANS turbulence closure. The fluid has a density of $\rho = 1.0$ kg/m^3 and a kinematic viscosity of 4.0×10^{-5} m^2/s. It enters the domain from the $-x$ face with a velocity of 120 m/s in the $+x$-direction. The airfoil has no-slip boundary conditions applied. All faces have an essential temperature BC set to 273.15 K, except for the $\pm z$ sidewalls and $+x$ outflow, which set natural temperature flux to zero. The outflow's essential pressure is set to 1×10^5 Pa. The $\pm y$ and $\pm z$ walls are inviscid and impenetrable.

To seek a steady solution, both LF and HF simulations are run at a fairly large time step of $\Delta t = 1 \times 10^{-2}$ s with first-order time integration until negligible solution change is observed between iterations, and the flow and scalar (eddy viscosity) solve absolute errors drop below 2×10^{-3} and 2×10^{-5}, respectively.

2.2 Mesh Generation and Deformation

The only distinguishing factor between the low- (LF) and high-fidelity (HF) runs is the mesh resolution; they use the following "coarse" and "fine" meshes, respectively.

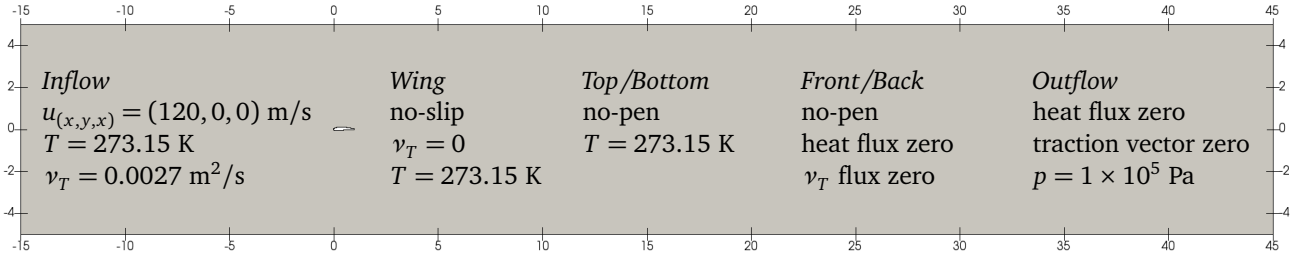

Figure 1: Schematic of computational domain with BCs listed. Spatial units in meters.

For both the LF and HF runs, we begin by meshing the fluid volume around a standard NACA 0012 airfoil at zero angle of attack, the outline of which is shown in Figure 2. This allows us to iterate the mesh until it adequately captures the airfoil's curvature.

Both coarse and fine meshes are created by extruding a mesh on the $+z$-face through the domain. Results are shown in Figures 4 and 3, respectively. Because geometric variation is central to this study, both meshes attempt to resolve airfoil curvature as well as possible. There are two main differences between the meshes: (1) the coarse mesh makes no attempt to resolve the shear layer downstream of the trailing edge, and (2) the fine mesh fully resolves the boundary layer (BL) with a first point off the wall at 2×10^{-6} m ($y^+_{\max} \sim 0.1$) and gradation factor of 0.8, whereas the coarse mesh has a first point off the wall at 0.01 m ($y^+_{\max} \sim 4 \times 10^4$) with the same gradation factor. The coarse mesh's y^+ is already well past the defect layer of a turbulent BL, and therefore has no hope of accurately capturing wall effects.

The converged NACA 0012 flow solution acts as the starting point for each new combination of geometric parameters we want to test. Geometric parameters are specified in an ASCII input file. Upon reading this file, PHASTA applies a displacement to each node on the surface of the airfoil, represented by the black lines in Figure 2. A linear elastic structural solver[1] satisfies the displacement constraints and deforms the entire mesh in accordance with the specified geometric parameters. Positive volumes on boundary layer elements are preserved by enforcing an inverse relationship between element volume and stiffness. As before, numerical solution of the flow equations proceeds until statistically-steady results are again obtained.

Each simulation uses randomly selected inputs within the allowed range for the geometric parameters, as specified in Table 1. When the simulation's stopping criterion is met, C_p information is extracted from the solution file through a ParaView script, and stored with an identifier linking the run to its geometric parameters.

For a given study of random parameter distributions, 1000 LF and 1000 HF runs are carried out. An interpolating decomposition (ID) is generated from the LF runs, and is used to determine which geometries contribute most to the variation in C_p (see Doostan et. al. 2016). A truncated ID including only the largest coefficients is then used to reconstruct the solution quantities of interest. Expansion coefficients from the ID of LF-origin are combined with their corresponding basis vectors, which now come from HF simulations.

TABLE TABLE TABLE

Table 1: Geometric parameters used in each of the three studies.

HF simulations are then run for only the select few geometric configurations with the largest ID coefficients. These HF simulations combine SA-RANS with large eddy simulation (LES) through dynamic detached-eddy simulation (DDES). Because they resolve unsteady shedding, the HF runs require time averaging, whereas the low-fidelity RANS simulations do not. The truncated ID is then used to reconstruct the solution quantities of interest: expansion coefficients from the ID of LF-origin are combined with their corresponding basis vectors, which now come from HF simulations.

To verify the accuracy of the bi-fidelity approach, more HF simulations are run using geometric configurations not present in the truncated expansion. The HF simulation results are compared to those predicted by the truncated bi-fidelity expansion.

[1] Courtesy of Eric Peters, University of Colorado at Boulder

3 RESULTS

The shape of a 4-digit NACA xyzz airfoil is specified by three geometric parameters, all non-dimensionalized with respect to the chord length c:

- $m = \mathrm{x}/100$ is the maximum camber
- $p = \mathrm{y}/10$ is the location of maximum camber
- $t = \mathrm{zz}/100$ is the maximum thickness

For a physical coordinate $x \in [0, c]$, the thickness of a symmetric airfoil is given by

$$y_t = 5tc\left[0.2969\sqrt{\frac{x}{c}} + (-0.1260)\left(\frac{x}{c}\right) + (-0.3516)\left(\frac{x}{c}\right)^2 + 0.2843\left(\frac{x}{c}\right)^3 + (-0.1015)\left(\frac{x}{c}\right)^4\right] \tag{1}$$

The coordinate pairs of points on the upper (x_U, y_U) and lower (x_L, y_L) surface are simply $x_U = x_L = x$, $y_U = y_t$, and $y_L = -y_t$. A symmetric airfoil corresponds to the NACA 00zz series. One example is NACA 0012, shown in Figure **??**.

Cambered NACA airfoils define thickness perpendicular to the camber line, which can be defined as

$$y_c = \begin{cases} m\frac{x}{p^2}\left(2p - \frac{x}{c}\right) & 0 \le x \le pc \\ m\frac{c-x}{(1-p)^2}\left(1 - 2p + \frac{x}{c}\right) & pc \le x \le c \end{cases} \tag{2}$$

The upper and lower coordinate pairs become

$$\begin{aligned} x_U &= x - y_t \sin\theta \qquad y_U = y_c + y_t \cos\theta \\ x_L &= x + y_t \sin\theta \qquad y_L = y_c - y_t \cos\theta \end{aligned} \tag{3}$$

where

$$\theta = \arctan\left(\frac{dy_c}{dx}\right) \quad \text{and} \quad \frac{dy_c}{dx} = \begin{cases} \frac{2m}{p^2}\left(p - \frac{x}{c}\right) & 0 \le x \le pc \\ \frac{2m}{(1-p)^2}\left(p - \frac{x}{c}\right) & pc \le x \le c \end{cases} \tag{4}$$

Because cambered profiles are generated from their symmetric counterparts, we can analytically determine the displacements necessary to deform any symmetric NACA mesh into an arbitrary 4-digit NACA mesh. This results in substantial efficiency gains. In our case, we create a CAD model of a NACA 0012 airfoil, mesh it, and partition it once. Then, in the initialization stage of a new simulation, we generate a stochastic NACA realization parameterized by random variables **m**, **p**, and **t**. Each mesh node on the airfoil surface is prescribed a displacement based on its x-coordinate, which is then passed to a linear elastic structural solver. Numerical solution of the unsteady incompressible Navier-Stokes equations proceeds on the deformed mesh.

4 CONCLUSION AND DISCUSSION

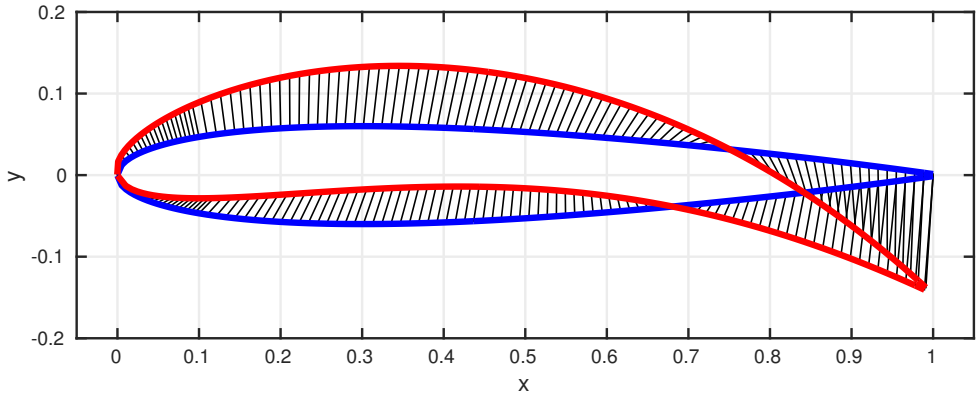

Figure 2: Deforming a NACA 0012 airfoil (blue) to an arbitrary NACA 4-digit airfoil (red). Point displacements indicated in black.

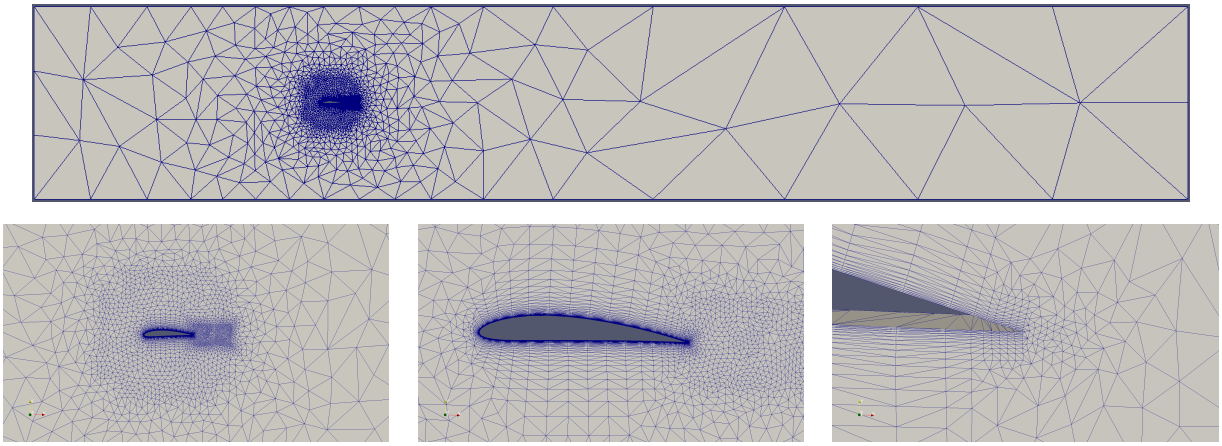

Figure 3: "Coarse" 2-D mesh of fluid domain around a NACA 4412 airfoil, containing approximately 5,500 tetrahedral elements. Counter-clockwise from top: zooming in from full domain to trailing edge of airfoil.

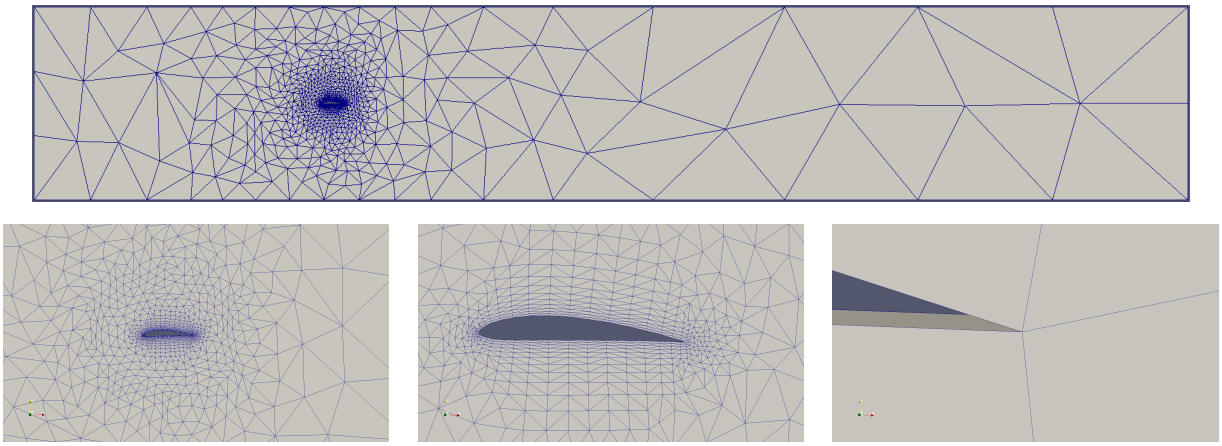

Figure 4: “Fine” mesh equivalent of Figure 3, containing approximately 32,000 tetrahedral elements.